Dependence of Shear and Concentration on Fouling in a Membrane Bioreactor with Rotating Membrane Discs

Mads K. Jørgensen, Malene T. Pedersen, and Morten L. Christensen
Dept. of Biotechnology, Chemistry and Environmental Engineering, Aalborg University, Sohngaardsholmsvej 57, DK-9000 Aalborg, Denmark

Thomas R. Bentzen
Dept. of Civil Engineering, Aalborg University, Sohngaardsholmsvej 57, DK-9000 Aalborg, Denmark

DOI 10.1002/aic.14302
Published online December 31, 2013 in Wiley Online Library (wileyonlinelibrary.com)

Rotating ceramic membrane discs were fouled with lab-scale membrane bioreactors (MBR) sludge. Sludge filtrations were performed at varying rotation speeds and in different concentric rings of the membranes on different sludge concentrations. Data showed that the back transport expressed by limiting flux increased with rotation speed and distance from membrane center as an effect of shear. Further, the limiting flux decreased with increasing sludge concentration. A model was developed to link the sludge concentration and shear stress to the limiting flux. The model was able to simulate the effect of shear stress and sludge concentration on the limiting flux. The model was developed by calculating the shear rate at laminar flow regime at different rotation speeds and radii on the membrane. Furthermore, through the shear rate and shear stress, the non-Newtonian behavior of MBR sludge was addressed. © 2013 American Institute of Chemical Engineers *AIChE J*, 60: 706–715, 2014
Keywords: activated sludge, non-Newtonian fluids, shear stress, apparent viscosity, ultrafiltration

Introduction

Membrane bioreactors (MBR) are an attractive alternative solution for municipal and industrial wastewater treatment. The technology combines a bioreactor for microbial degradation of sludge components and a membrane filtration unit, either submerged or in a sidestream configuration, for separation of the sludge.[1,2] Compared to conventional systems, MBR systems have a low footprint, can handle higher sludge concentrations and, most important, give clearer effluent with no bacteria present in the permeate. However, the limitation of the membrane filtration process is membrane fouling.[1,2] The accumulation of sludge components on membranes gives a lower permeability of the sludge. Hence, at constant pressure filtration, the flux declines over time and productivity decreases.

To recover permeability physical and chemical cleaning is applied over time. Physical cleaning removes the removable fouling layers (often cake layers) by relaxation, enhanced shear (by either air scouring or crossflow) or backwash.[1,2] The irremovable fouling, often described as pore blocking, adsorbed macromolecules or gel layer, is removed by chemical cleaning, before eventually replacing the membranes due to irreversible fouling[2] and damage of the membranes.

Several studies have been conducted to limit and predict membrane fouling at different operating conditions. One effective and easy way to limit fouling of MBRs is to increase shear, as shear removes fouling and is easy for operators to control. Therefore, studies have focused on the effect of shear on flux and decline in permeability during MBR filtrations.[3–9] However, findings are often limited to apply for the individual MBR system at given operational conditions. Therefore, a more general understanding of the influence of shear on flux is needed.

To give a more universal understanding of fouling, the formation of fouling layers can be described with a mass-balance approach.[10,11] In the one-dimensional (1-D) mass balance, Eq. 1, the product of the permeate flux (J) and the sludge volume fraction (ϕ) composes the permeation drag, dragging particles toward the membrane surface. The back transport of foulants is affected by chemical interactions between foulants and membrane and foulant-foulant interaction $p(\zeta)$, Brownian diffusion (D_B), and shear-induced diffusion (D_S). Therefore, a mass balance for the development in amount of fouling can be written as

$$\frac{d\omega}{dt} = J \cdot \phi - D_S \frac{d\phi}{dx} + D_B \frac{d\phi}{dx} + p(\zeta) \tag{1}$$

The impact of each of those mechanisms on back transport depends on the type of foulant. Brownian diffusion increases with lower particle size, hence smaller colloids and molecules can have significant back transport due to Brownian diffusion.[10] Conversely, particles and larger colloids are more exposed to shear-induced diffusion compared to, for example, smaller colloids and macromolecules.[10] Finally, macromolecules and colloids tend to form comprehensive and to some extent irremovable fouling layers, due to chemical interactions caused by, for example, surface charges.[10]

Correspondence concerning this article should be addressed to M.K. Jørgensen at mkj@bio.aau.dk.

Previous studies have shown that from the mass balance in Eq. 1, the development in fouling can be simulated.[12,13] In these studies, fouling in short-term experiments are considered as an effect of cake formation, controlled by the mass balance, and cake compression. The limiting flux, J_{LIM}, has been described as the pressure-independent steady-state flux, above which the flux will always decline to the same value,[10,12] as it is the mass transport in Eq. 1 that determines the flux level. Therefore, the back transport term in the mass balance is reduced to $J_{LIM} \cdot \phi$. Hence, increasing shear will result in higher limiting flux and lower decline in flux due to fouling. In agreement with this, Aubert et al.[8] has shown that on a rotating membrane disc, the back transport increases with shear stress on the membrane or cake surface due to shear-induced erosion, which leads to a lower decline in flux.

Studying the influence of shear in MBR systems are complicated by the complexity of shear generated in multiphase systems. However, with membrane discs, the shear can be manipulated by varying the rotation speed or the radial distance of the areas of the disc open for filtration.[8,9,14,15] Some MBR systems use membrane rotation to reduce fouling, others static membranes with impeller generated crossflow. To characterize the efficiency of membrane rotation to prevent fouling, the present study will find the influence of shear in limiting flux in a MBR system with rotating membrane discs. This is done by developing a model to describe the dependency on shear stress and concentration on the limiting flux and compare this model, with experimental data for flux at varying concentration, radial distance on the membrane, and rotation speed.

Theory

Background

The combination of a concentration gradient of foulants and shear along a membrane gives a back diffusion of foulants.[16–18] This can be described from Figure 1.

The figure can be described from the following mass balance for equilibrium; hence the permeation drag equals the back transport, if total reversibility of fouling is assumed ($p(\zeta) = 0$)

$$J_{LIM}\phi = D\frac{d\phi}{dx} = (D_S + D_B)\frac{d\phi}{dx} \tag{2}$$

Where $J \cdot \phi$ is the transport of foulants toward the membrane, ϕ is the volume fraction of particles (relative to concentration), x is the distance from membrane surface, and D is the diffusion coefficient covering both shear-induced diffusion (D_S) and Brownian diffusion (D_B). The boundary conditions for the mass balance is, that if $x = 0$, then $\phi = \phi_w$ and when $x = \delta$ (the boundary layer thickness), then $\phi = \phi_b$. Hence, the greater difference between concentration near the membrane wall and concentration in bulk, the higher back transport. However, at some point, the volume fraction of particles at the membrane reaches a maximum, $\phi_{w,max}$, corresponding to a maximum packing density of particles. Hence, when a cake has formed, there is a constant ϕ_w, hence if ϕ_b is constant the back transport is constant as well. Furthermore, the concentration gradient is no longer a function of concentration at the surface of the membrane, but a function of the concentration at the surface of the cake, hence the thickness of the boundary layer, δ, is the same but

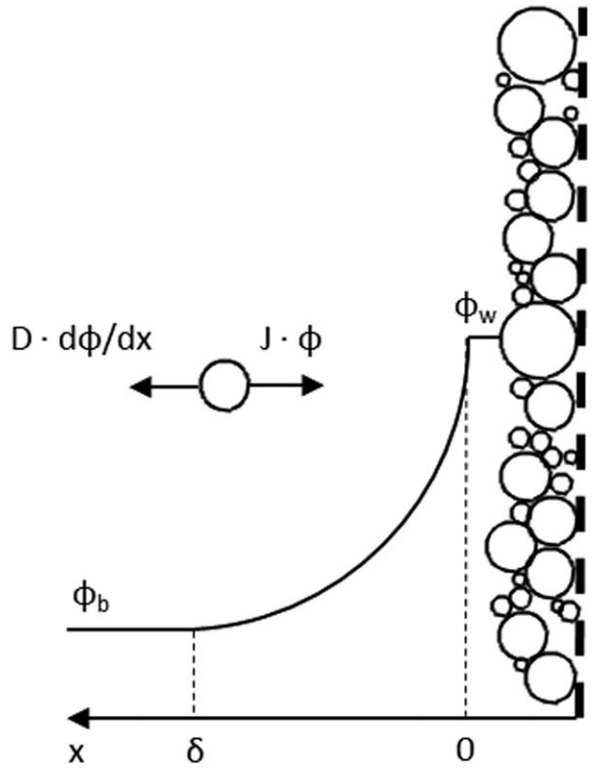

Figure 1. Concentration profile of foulants near a fouled membrane and 1-D permeation drag and diffusion.

does no longer start from $x = 0$. Several studies show, that $\phi_{w,max}$ is given as a constant value around 0.58–0.62.[16] The boundary layer thickness is a function of feed concentration and the velocity profile, hence shear stress.

The shear-induced diffusion coefficient, D_s, is a function of shear rate and radius of foulants. The following empirical relationship has been developed by Leighton and Acrivos[19] by introducing a dimensionless hydrodynamic diffusion coefficient, $\hat{D}(\phi)$

$$D_S = \dot{\gamma}_m a^2 \hat{D}(\phi), \text{ where } \hat{D}(\phi) = 0.33\phi^2\left(1 + 0.5e^{8.8\phi}\right) \tag{3}$$

Where a is the particle radius and $\dot{\gamma}_m$ is the shear rate on the membrane. In the case of particle/sludge deposition on a membrane in MBR, the Brownian diffusion will be assumed to be negligible. Hence, only the shear-induced diffusion will be considered. Solving the mass balance with the above boundary conditions and implementing Eq. 3 gives

$$J_{LIM} = \frac{\dot{\gamma}_m a^2}{\delta}\int_{\phi_b}^{\phi_w}\frac{\hat{D}(\phi)}{\phi}\cdot d\phi \tag{4}$$

From here, several attempts have been done, to understand the shear influence on back transport from crossflow velocity/shear, concentration of foulants, and viscosity of the feed stream in membrane filtration.

One widely accepted model for shear-induced diffusion is developed by Davis and Sherwood,[16] by considering 2-D movement of particles a result of shear-induced diffusion, axial movement from crossflow and permeation drag. The axial movement of "mobile cake" gives a change in thickness of fouling layer along the axial direction in the membrane module. This model will not be valid to describe flux

in a MBR using rotating membrane discs for two reasons. First, on a rotating membrane disc, the boundary layer thickness will not vary along the axial direction, as it will return to the same position again and again. Hence, at a given radius from the center of rotation, r, the boundary layer thickness and cake height will be constant. Furthermore, the wall shear rate on a rotating disc will increase with r, as the velocity increases with radius. Second, in several studies, activated sludge and MBR sludge have been shown to be non-Newtonian,[20–23] which give a nonlinear response of shear stress to shear rate.

Relation of shear and concentration to flux in MBR

Accepting that sludge is a complex mixture with heterogeneity of foulants, a flux model is not proposed from an analytical solution by integration from Eq. 4. Instead an empirical model is proposed to describe the flux on a rotating disc as a function of rotation speed, radial distance and sludge concentration. This is done with emphasis on the following key parameters influencing back transport in membrane filtration based on the findings of the previous section:

- Sludge concentration[4,6]
- Shear stress. Several studies has shown that the fouling rate and thereby limiting flux depends on shear stress and shear rate,[3,7,8,24–27]

Shimizu et al.[6] proposed an empirical model for the limiting flux in MBR to have the form

$$J_{\mathrm{LIM}} = A \cdot u^{*} \cdot \varphi \cdot \mathrm{TSS}^{-1/2} \tag{5}$$

A is a filtration constant that describes the sludge filtration characteristics, u^{*} is the superficial air velocity creating shear, φ is the geometric hindrance factor, and TSS is the total suspended solids concentration. In accordance with Eq. 4 and the mass balance in Figure 1, higher sludge concentration gives lower J_{LIM}, as the gradient for shear-induced diffusion decreases with concentration. Furthermore, the limiting flux shear dependency is accounted for with the superficial air velocity.

In the present study, the effect of shear is described from the shear stress, τ_m, rather than an air velocity. The limiting flux increases with shear stress, as the back transport is promoted by shear, as derived from Eq. 4. Several shear-dependent back transport mechanisms can occur for foulants near a membrane in MBR: Shear-induced diffusion (especially particles and large colloids), Brownian diffusion (small colloids and macromolecules), cake erosion, lateral migration, and so forth.[26,27] As sludge is a complex mixture, we cannot rule out any of these mechanisms.

The relationship between J_{LIM} and shear stress has been reported to be linear in some cases for shear-induced diffusion,[26] lateral migration,[26] and shear erosion,[8] whereas for Brownian diffusion,[26] J_{LIM} is linearly proportional to $\tau_m^{1/3}$. Furthermore, the boundary layer thickness is also a function of shear stress and decreases with higher shear stress and lower sludge concentration.[24] However, the boundary layer thickness is not only a function of the shear generated by the disc rotation but also depends on the streaming of fluid from the center of the membrane and out. The combination of these shear depending factors can result in nonlinearity between J_{LIM} and τ_m.

The net effect of shear rate and shear stress has been observed to be nonlinear for some studies.[14,28,29] The nonlinearity between the flux and shear rate is observed by the flux starting to level out at high shear levels. This has been explained to be caused by the membrane becoming free of fouling at high shear, whereby the impact of enhanced shear will be limited.[28] Other studies have found empirical models, where J_{LIM} depends on τ_m^{B} with the exponent B accounting for the effect of module geometry on the effect of shear stress.[30,31]

Accepting that the influence of shear stress on the back transport and thereby limiting flux may be an effect of several parameters and module configuration, an empirical exponent, B, for the shear stress, is introduced to compensate for the influence of several shear depending factors in the complex disc module. Therefore, a model, of the form as given in Eq. 6, is suggested.

$$J_{\mathrm{LIM}} = A \cdot \tau_m^{B} \mathrm{TSS}^{-1/2} \tag{6}$$

A is a filtration constant that depends on the sludge mixtures response to shear near the membrane, as described by Shimizu et al.[6] Therefore, it depends on sludge characteristics such as particle size and particle-size distribution, in accordance with the particle-size effect describe in Eq. 4. The exponent B will describe the effect of shear accounting for the module geometry and effect of several shear depending back transport mechanisms. The model has the properties that J_{LIM} decreases with sludge concentration, which is in agreement with the lower concentration gradient promoting lower back transport. Furthermore, the limiting flux increases with increasing shear stress, which is in agreement with Eq. 4.

Shear rate on a rotating membrane disc in sludge

To address the distribution of shear on a flat rotating membrane disc, the shear rate is calculated. The following equations are valid for calculating the shear rate on the surface of a rotating flat membrane disc at laminar and turbulent flow regimes, respectively.[14,15,29]

$$\dot{\gamma}_m = 1.81 \upsilon^{-0.5} (k\Omega)^{1.5} r \tag{7a}$$

$$\dot{\gamma}_m = 0.057 \upsilon^{-0.8} (k\Omega)^{1.8} r^{1.6} \tag{7b}$$

v is the kinematic viscosity of the feed suspension, r is the radius, hence distance from the center of rotation, and Ω is the rotation speed (rad s^{-1}). The velocity factor $k = 0.42$ applies for a flat rotating disc.[29] Integrating Eq. 7a over the membrane disc with inner and outer radius, r_i and r_o gives

$$\dot{\gamma}_m = 0.5133 \upsilon^{-0.5} (k\Omega)^{1.5} \frac{r_o^3 - r_i^3}{r_o^2 - r_i^2} \tag{8}$$

As sludge is a non-Newtonian fluid, the viscosity depends on the sludge concentration and the shear rate. Rosenberger et al.[23] has described the apparent dynamic viscosity (mPa·s) of sludge to have the following form.

$$\mu_a = \exp\left(2\mathrm{TSS}^{0.41}\right) \dot{\gamma}^{-0.23\mathrm{TSS}^{0.37}} \tag{9}$$

Therefore, with higher concentration the viscosity increases, while higher shear gives lower sludge viscosity (shear thinning). The kinematic viscosity (m^2 s^{-1}) of the sludge can then be calculated from

$$\upsilon = \frac{\mu_a}{1000 \rho_{\mathrm{s}}} \tag{10}$$

where $\rho_{\mathrm{s}} = 1040$ kg m^{-3} is the sludge density. Inserting Eqs. 9 and 10 into Eq. 8 gives

$$\dot{\gamma}_m = 0.5133\left(\frac{1}{1000\rho_s}\exp\left(2\mathrm{TSS}^{0.41}\right)\dot{\gamma}_m^{0.23\mathrm{TS}^{0.37}}\right)^{-0.5}(k\Omega)^{1.5}\frac{r_o^3-r_i^3}{r_o^2-r_i^2} \tag{11}$$

which can be rewritten to give

$$\frac{\dot{\gamma}_m}{\dot{\gamma}_m^{0.115\mathrm{TS}^{0.37}}} = \dot{\gamma}_m^{1-0.115\mathrm{TS}^{0.37}} = 0.5133 \left(\frac{1}{1000\rho_s}\exp\left(2\mathrm{TSS}^{0.41}\right)\right)^{-0.5}(k\Omega)^{1.5}\frac{r_o^3-r_i^3}{r_o^2-r_i^2} \tag{12}$$

and

$$\dot{\gamma}_m = \left(0.5133\left(\frac{1}{1000\rho_s}\exp\left(2\mathrm{TSS}^{0.41}\right)\right)^{-0.5}(k\Omega)^{1.5}\frac{r_o^3-r_i^3}{r_o^2-r_i^2}\right)^{1/1-0.115\mathrm{TS}^{0.37}} \tag{13}$$

This equation should be valid for calculating the shear rate on a flat membrane rotating in MBR sludge with a concentration, TSS, at laminar conditions. For turbulent conditions, the shear rate can be solved to give

$$\dot{\gamma}_m = \left(0.0164\left(\frac{1}{1000\rho_s}\exp\left(2\mathrm{TSS}^{0.41}\right)\right)^{-0.8}(k\Omega)^{1.8}\frac{r_o^{3.6}-r_i^{3.6}}{r_o^2-r_i^2}\right)^{1/1-0.184\mathrm{TS}^{0.37}} \tag{14}$$

Flow regime

Reynolds number is calculated to decide if the flow regimes are laminar or turbulent. Reynolds number is determined from the following equation.[32,33]

$$Re = \frac{k\Omega r^2}{v} \tag{15}$$

The viscosity of sludge determined from Eq. 9 accounting for the non-Newtonian behavior of the sludge is used to determine Reynolds number at different membrane rotation speeds and radii. If $Re < 4.5{\cdot}10^4$, then the flow regime is laminar, and at $Re > 2{\cdot}10^5$, the flow is turbulent. The transition from laminar to turbulent flow regime occurs in the range $4.5{\cdot}10^4 < Re < 2{\cdot}10^5$.

Shear stress

As sludge is a non-Newtonian liquid, there is not a linear relationship between the shear stress and shear rate. Instead, the wall shear stress induced by a shear rate on MBR sludge is calculated from the following equation[20,21,23]

$$\tau = m\dot{\gamma}^n \tag{16}$$

where m is the fluid consistency index and n is the flow behavior index ($n < 1$), both parameters depending on TSS

$$m = 0.001\exp\left(2\mathrm{TSS}^{0.41}\right) \tag{17a}$$

and

$$n = 1 - 0.23\mathrm{TSS}^{0.37} \tag{17b}$$

In Figure 2, Eqs. 13 and 14 are used to calculate the variations of shear rate and shear stress at different concentrations and radii on a membrane with $r_i = 0.045$ m and $r_o = 0.155$ m and rotation speeds in the range 100–280 rpm.

The figure shows higher shear rate and shear stress with rotation speed. The shear rate increases exponentially with radial distance, while the shear stress has a more linear form, due to the pseudoplastic behavior of the sludge. Also Figure 2c shows higher shear rate at lower concentration of sludge, while the shear stress increases with sludge concentration. This corresponds to findings in Rosenberger et al.[23] and Ratkovich et al.[33]

Experimental

Filtration system

For filtration experiments, a sidestream filtration system, further described in Jørgensen et al.,[12] was connected to a MBR with 350 L activated sludge from the Aalborg East Wastewater Treatment Plant. The reactor was fed with a synthetic substrate of dogs food and fish meal, to reach a food to microorganism ratio (F:M ratio) of 0.1.

MBR sludge characterization

The TSS concentration was determined by measuring the weight gain of a filter paper (47 mm, 0.6 μm, GA-55, Advantec, Japan) after filtration of a given sludge volume. The sludge pH and conductivity was measured with a pH-meter (PHM 290, Radiometer Analytical, France) and a conductivity-meter (CDM 210, Radiometer Analytical, France), whereas the particle size was determined with a Microtrac (MICROTRAC II Particle size analyzer model no. 7997-10, Leeds & Northrup, UK).

The capillary suction time (CST), which is closely related to the filtration properties of sludge, was measured (304B CST, Triton Electronics, UK). The residual turbidity was determined by measuring the turbidity of supernatant at 650 nm (Helios Epsilon, Thermo Spectronic) from a 5 mL sludge sample centrifuged for 2 min at 3000 rpm (Model 1–6, Sigma Laboratory Centrifuges, Germany). The sludge characteristics are summarized in Table 1.

Procedure for filtrations

At all filtrations, the recirculation through the 30 L filtration system was kept in the range of 1–2 L min^{-1}, to keep the hydraulic retention time in the reactor low (15 min). The limiting flux, J_{LIM}, was determined with a modeling approach on transmembrane pressure (TMP)-step experiments presented in Jørgensen et al.[12] Two set of filtration experiments were carried out; Filtrations on different concentric rings of membranes and filtrations at varying sludge concentrations. Common for the experiments was, the applied ZrO_2 ultrafiltration (UF) membranes with an average pore diameter of 60 nm (KERAFOL Keramische Folien GmbH, Eschenbach, Germany).

Determination of limiting flux

A model was fitted to the flux measured at different pressures obtained from TMP-step experiment to determine the limiting flux with the following modeling approach, adopted from Jørgensen et al.,[12] to determine J_{LIM}. The model assumes reversible cake buildup and compression. The amount of cake, ω_c, is modeled numerically with an Euler approach with the following equation

$$\omega_{c,t} = \omega_{c,t-1} + \frac{d\omega_c}{dt}\Delta t = \omega_{c,t-1} + (J_t - J_{\mathrm{LIM}})\mathrm{TSS}\cdot\Delta t \tag{18}$$

The mass balance for the development in cake is in principle the same as the Eq. 1, where the sum of the back transport is described with J_{LIM}. The time step was set to Δt = 1 s. From the pressure drop over the cake, the pressure-dependent specific cake resistance, α, is determined

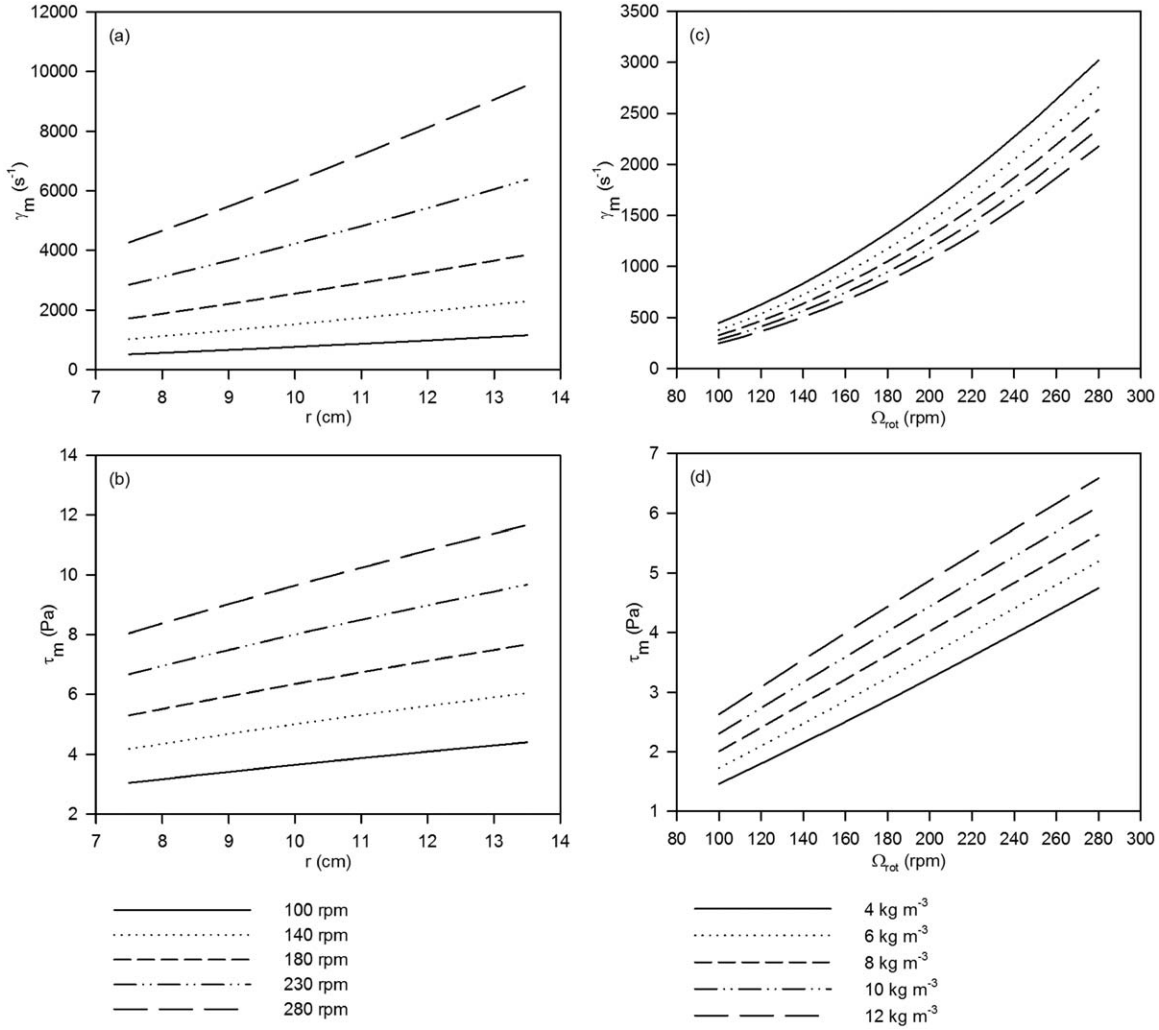

Figure 2. Shear rate (a) and shear stress (b) as function of radial position and shear rate (c) and shear stress (d) as function of rotation speed at different sludge concentrations on a full membrane.

$$\alpha = \alpha_0 \left(1 + \frac{\Delta P_c}{P_a}\right) \tag{19}$$

The pressure drop over the membrane is calculated from $\Delta P_c = \text{TMP-}J \cdot R_m \cdot \mu$. α_0 is the specific cake resistance at no pressure, while P_a is the pressure required to obtain a specific cake resistance twice as high as α_0.

The flux over time can then be modeled from the TMP, amount of cake and the specific cake resistance, by use of the Darcy equation

$$J = \frac{\text{TMP}}{\mu(R_m + \alpha \cdot \omega_c)} \tag{20}$$

R_m is found for pure water filtration to be $1.8 \cdot 10^{12}$ m^{-1}. This flux will decline over time to converge toward J_{LIM} with kinetics depending on J_{LIM}, due to the cake buildup dependency of J_{LIM}. Therefore, the modeled flux can be fitted to the measured flux in the pressure step experiments, by fitting J_{LIM}, α_0 and P_a to obtain the lowest total root mean square error. Doing this for step experiments at different operating conditions gives J_{LIM} characteristic to these operating conditions. The modeling approach is further described in Jørgensen et al.[12]

Filtrations on different concentric rings of membranes

Five different membrane samples were prepared to study the radial distribution of flux. One full membrane and four partly "blinded" membranes, illustrated in Figure 3, were used for TMP-step experiments. The TMP-step experiments were performed at 61, 100, 150, 200, and 250 rpm to determine the flux at different areas of the discs and the rotation speeds impact on this distribution. The filtrations were performed on 11 kg m^{-3} MBR lab-scale sludge.

Table 1. Characteristics of MBR Sludge Used for Filtration Experiments

MBR Sludge	pH	Conductivity (μS cm^{-1})	CST (s)	TSS (kg m^{-3})	Residual Turbidity	Particle Size (μm)
Filtrations on different membranes	7.83	922	173	11	0.399	41
Filtrations at varying concentrations	7.48	1011	202	4.7, 10, 12.7	0.297	64

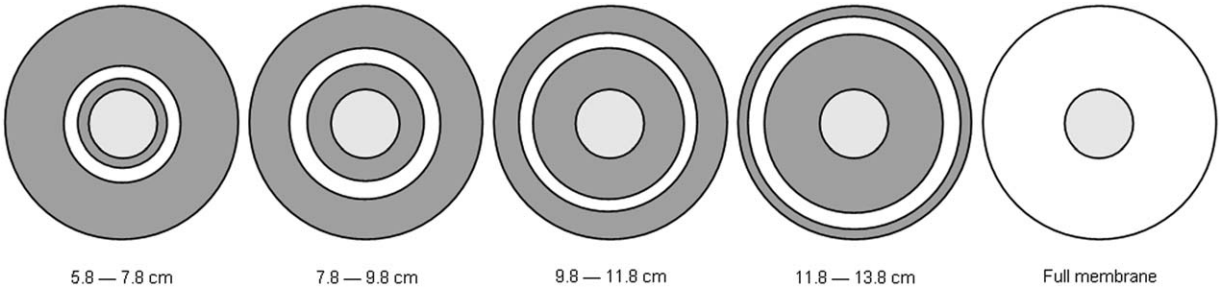

Figure 3. Illustration of membranes used for filtration.

Gray zones of the membrane represent zones where the membrane has been blocked and thereby only allow filtration in the white 2-cm-thick rings.

The four partly blinded membranes was covered with an impermeable coating (Scotch-clad 776 Protective Coating, 3M, France) except from some 2-cm-thick concentric rings at radial distances 5.8–7.8, 7.8–9.8, 9.8–11.8, and 11.8–13.8 cm, respectively, that were kept open for filtration. The membrane permeability of each blinded disc was found to correlate with the permeability of a full disc, which shows that the coating was able to blind the different areas of the discs. For each filtration, one of the membranes was placed in the filtration cell and connected to the motor for rotation.

Due to the low flow through the permeable areas of the blinded membranes, the permeate flux was determined by logging the weight (Balance: PB3002-L, Mettler Toledo) of a beaker collecting permeate. Permeate was transferred back to the bioreactor to keep the sludge conditions constant. The flux was measured at each pressure over 20 min until a cake was developed and flux reached a steady state.

Filtrations at varying concentrations

TMP-step experiments were carried out in the pressure range of 0.3–2.5 bar.[12] At the different pressures, the flow was logged with a flowmeter (Magflowmeter type 8051, Bürkert, Germany). Two ceramic ZrO_2 membranes with an average pore diameter of 60 nm were placed in the filtration cell and connected to the motor for membrane rotation. During the filtration experiments at constant pressure, the flux reached a steady state, hence the cake was developed.

TMP-step experiments were conducted on rotation speeds in the range 100–280 rpm at three different concentrations; 4.7, 10, and 12.7 kg m^{-3}. The 4.7 kg m^{-3} sludge suspension was obtained by diluting 10 kg m^{-3} sludge suspension from the MBR lab-scale reactor with supernatant from settled sludge. This was done to keep the conductivity constant to avoid deflocculation of the sludge flocs when diluting the sludge. The 12.7 kg m^{-3} sludge suspension was prepared by settling a 10 kg m^{-3} lab-scale MBR sludge suspension and removing the supernatant.

Results and Discussion

Radial Reynolds number

Reynolds number is calculated from Eq. 15 to determine the flow regime on the disc. The kinetics of sludge with TSS = 11 kg m^{-3} was determined from Eqs. 9 and 10. The shear rate used to determine the apparent viscosity was calculated from the laminar expression for shear rate in Eq. 13.

Figure 4 shows Reynolds numbers calculated at different areas of the partly blinded membranes and as function of rotation speed. The Reynolds number increases with rotation

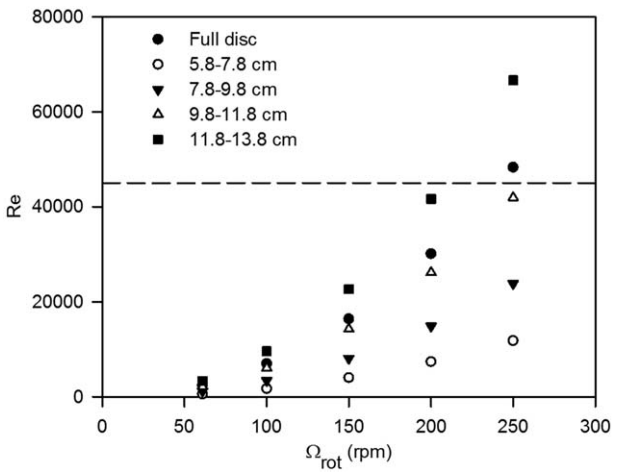

Figure 4. Reynolds number vs. rotation speed at different concentric rings of the membrane and one full membrane disc.

The dashed line represents the limit for laminar flow regime, $Re = 4.5 \cdot 10^4$.

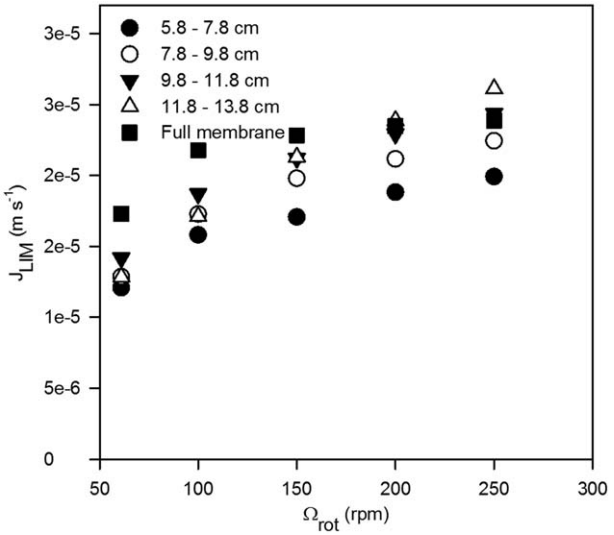

Figure 5. Limiting flux vs. rotation speed on a full membrane disc and a membrane discs with filtration enabled at different distances from the center of rotation.

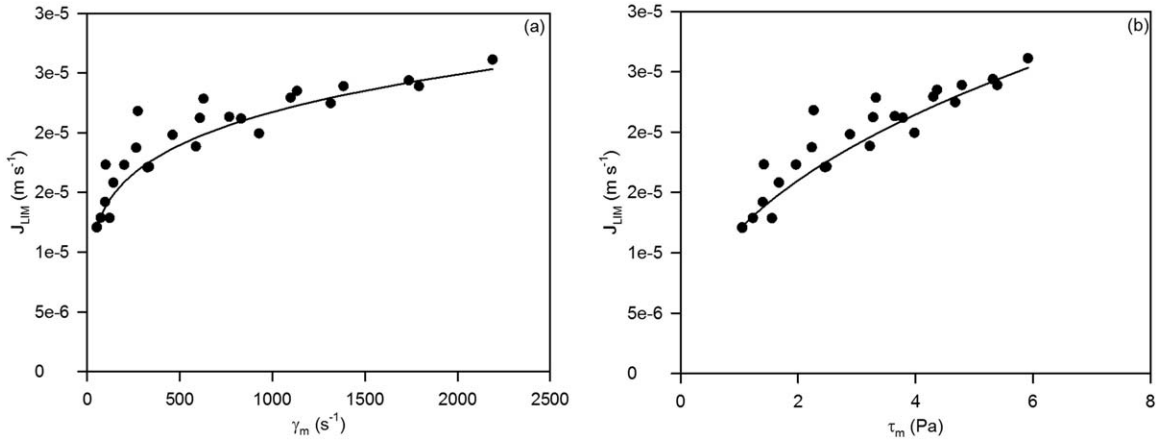

Figure 6. Experimental (points) and modeled (line) J_{LIM} vs. shear rate (a) and shear stress (b) at TSS = 11 kg m^{-3}.

J_{LIM} is modeled with Eq. 6 using the model parameters $A = 3.77 \cdot 10^{-5}$ kg$^{0.5}$·m$^{-0.5}$ s^{-1} and $B = 0.42$.

speed and radial distance from the center of the membrane, which is in accordance with the higher azimuthal velocity.

Furthermore, Figure 4 shows that all data points except two are below the limit for laminar flow regime, and none of the Reynolds numbers exceeds the limit for turbulent flows. Only two points are within the lower end of the transition between laminar and turbulent flows. Calculating the shear rate for turbulent flow and using this to determine the apparent viscosity and Reynolds number does not give a significant change of these results. The same two data points are still in the lower end of the transition range between laminar and turbulent flows. Therefore, it has been assumed, that the flow regime is laminar and that the shear rates calculated from Eq. 13 are valid for the operating conditions of the filtration experiments.

Flux dependency of radial distance and rotation speed

The limiting flux was determined at a full membrane and four partly blinded membranes with filtration enabled in the radial zones: 5.8–7.8, 7.9–9.8, 9.8–11.8, and 11.8–13.8 cm. The limiting flux determined for each membrane at rotation speeds 61–250 rpm at each ring is plotted in Figure 5.

The figure shows a trend, that the flux increases with rotation speed and with radius. This is consistent with the higher shear and, therefore, higher back transport of particles with higher azimuthal velocity. It can be expected that higher rotation speeds than the ones used in the present study will lead to higher J_{LIM} and, therefore, less fouling. However, due to high energy consumptions associated with membrane rotation in non-Newtonian fluids, membrane rotation speeds for MBR purposes are typically in the range applied in this study.[22,33]

There is some inconsistency with respect to the full membrane, as this shows a higher limiting flux at rotation speeds 61–150 than the membranes with filtration enabled from 11.8 to 13.8. This was unexpected, as the shear rate and shear stress is lower for the full membrane than at 11.8–13.8 cm from the center of rotation. In Bouzerar et al.,[14] inconsistency between the radial distribution of flux and the flux averaged over a full membrane disc was also found, as the

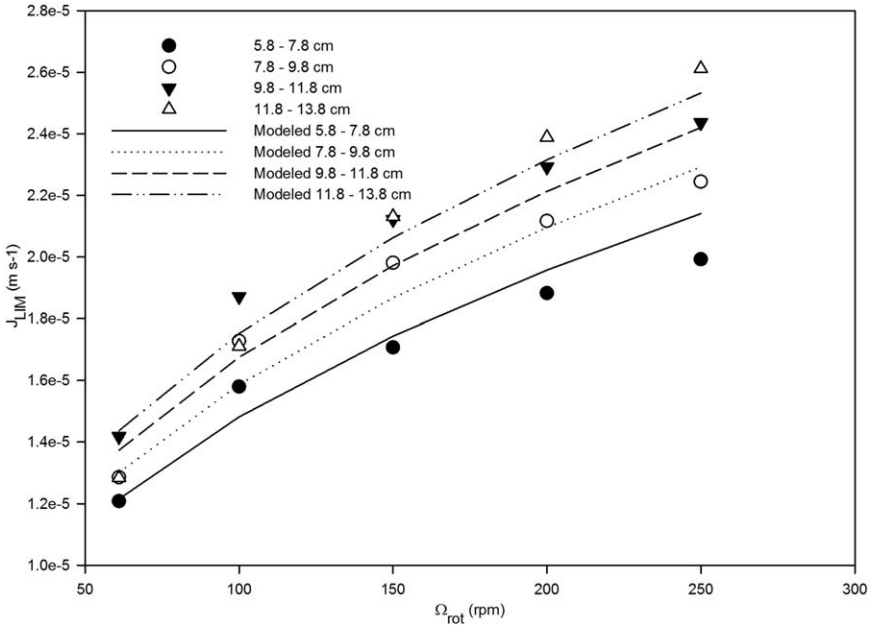

Figure 7. Modeled and experimental limiting flux vs. rotation speed for different concentric rings of the rotating membrane.

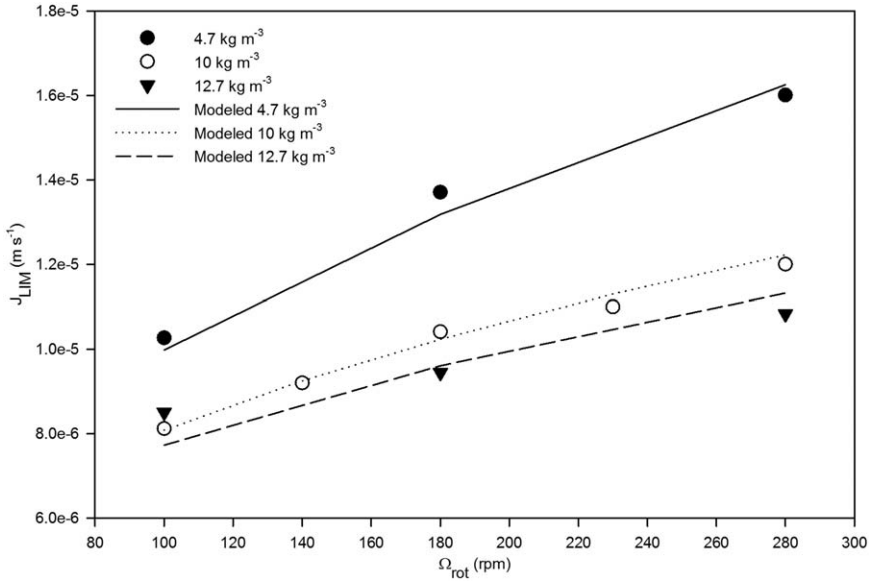

Figure 8. Experimental and modeled limiting fluxes vs. rotation speed at different sludge concentrations.

Limiting flux is modeled with Eq. 6 using the model parameters $A = 1.79 \cdot 10^{-5}$ kg$^{0.5}$·m$^{-0.5}$ s^{-1} and $B = 0.42$.

full membrane disc was shown to have the same flux as the inner concentric ring, hence the part of the membrane with the lowest shear. This, together with the results of the present study, can indicate that the assumption that the averaged shear stress over the entire membrane is comparable to the average flux over the membrane is wrong.

J_{LIM} is calculated from the proposed model in Eq. 6 and fitted to the experimental data. This gave a close fit between experimental and modeled data ($R^2 = 0.98$) with $A = 3.77 \cdot 10^{-5}$ kg$^{0.5}$·m$^{-0.5}$ s^{-1} and $B = 0.42$. Experimental and modeled J_{LIM} is plotted vs. shear rate and shear stress in Figure 6.

The figure shows increasing J_{LIM} with increasing shear rate and shear stress. The figure also shows a nonlinear relation between the experimental obtained limiting fluxes and the shear rate and shear stress. When converting the shear rate to shear stress with Eq. 6, the flux shear curve becomes more linear. The nonlinearity between J_{LIM} and shear stress is described through the exponent, B. According to Eq. 6 and 16, the J_{LIM} as function of shear rate with the following relationship

$$J_{LIM} = A \cdot m \cdot \gamma_m^{n \cdot B} \mathrm{TSS}^{-1/2} \tag{21}$$

With $n < 1$ the total exponent of the shear rate is lower than the exponent of the shear stress, which is in correlation with the observations of Figure 6.

The radial distribution of experimental compared with modeled J_{LIM} in the concentric parts of the concentric membrane rings is presented in Figure 7.

The figure shows that the model can simulate the development in flux through the different concentric rings of the membrane and the impact of enhanced rotation speed on the flux level.

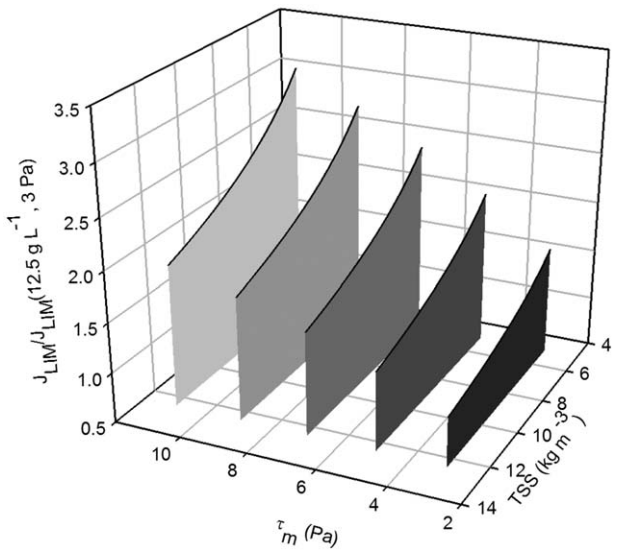

Figure 9. Normalized modeled limiting flux vs. shear stress and sludge concentration.

Flux dependency of sludge concentration

The limiting flux has been determined on a full membrane disc at three different sludge concentrations (4.7, 10, and 12.7 kg m^{-3}) and varying rotation speeds. The modeled flux determined from Eq. 6 was fitted to the experimental data by changing A, but keeping the exponent B constant. The result of the fitting process was a close fit to the experimental data with $R^2 = 0.975$, $A = 1.79 \cdot 10^{-5}$ kg$^{0.5}$·m$^{-0.5}$ s^{-1}, and $B = 0.42$. Experimental and modeled J_{LIM} at different concentrations with varying rotation speed is presented in Figure 8.

The figure shows, that higher rotation speeds gives higher J_{LIM}, consistent with the trend in Figure 7. Furthermore, the figure shows a higher J_{LIM} with lower sludge concentration. However, the shear stress is lower at lower concentrations (Figure 2d), though, and can, therefore, be expected to give a lower J_{LIM} with lower concentration. However, the proposed model, Eq. 6 seems to compensate this effect with the exponent, B, and the TSS$^{-1/2}$ term, and, therefore, also represents the effect of sludge concentration well.

The empirical parameter covers the overall filtration properties of the sludge suspensions and is a combination of different parameters, for example, particle size and particle-size distribution. For the experiments with varying sludge

concentrations, the sludge shows lower filtration properties through a lower value of A, compared to the sludge used in experiments studying the radial distribution of flux. This is in agreement with a higher CST value, indicating lower filterability of the sludge. However, it is in contrast to the higher particle size, as observed from Table 1, as larger particle sizes are expected to give higher shear-induced diffusion.[26] However, as the parameter A is a combined effect of different parameters, it covers the overall filterability of the sludge and not only particle size.

It should be noted, that the same exponent can represent the dependency of shear stress on limiting flux in the two series of experiments, although they were carried out at two different types of sludge. Therefore, B, is believed to represent the influence of shear stress on the net back transport mechanisms while the constant A seems to represent how the individual sludge with given characteristics (particle size distribution (PSD), etc.) is affected by a given level of shear. This is in agreement with the description by Moll et al.,[31] that B describes the geometry of the filtration module rather than the feed suspension characteristics. In Field and Wu,[34] the limiting flux has also been described to depend on shear stress with an exponent of 0.5, close the exponent of 0.42 found in the previous study. Jönsson[28] explained the nonlinearity was explained to be a consequence of the membrane becoming free of fouling at high shear levels, whereby the impact of enhanced shear will be limited. This may not be the case in this study, as the flux still declines throughout the filtration experiments and is significantly different from the pure water flux, approximately $3.3{\cdot}10^{-5}$ m s^{-1}. Instead, the nonlinear relationship between limiting flux and shear stress is a consequence of the complex effect of shear given the geometries of the filtration module. However, it cannot be ruled out that at lower shear levels, there may be linearity between limiting flux/back transport and shear.

From the fitted model parameters from Figure 8 ($A = 1.79{\cdot}10^{-5}$ $kg^{0.5}{\cdot}m^{-0.5}$ s^{-1} and $B = 0.42$), J_{LIM} is modeled for TSS in the range 5–12.5 kg m^{-3} and τ_m ranging 3–11 Pa are calculated and normalized with the flux at 12.5 kg m^{-3} and 3 Pa, J_{LIM} (12.5 kg m^{-3}, 3 Pa) and presented in Figure 9. The flux can be normalized as the empirical parameter, A, depends on sludge characteristics of the individual system. Therefore, the figure should represent the influence of rotation speed and sludge concentration on limiting flux in a high-shear MBR.

It is observed, that the flux in general increases with rotation speed and decreases with TSS. Increasing the shear stress from 3 to 9 Pa gives a 73–174% higher J_{LIM} for TSS 12–4 kg m^{-3} (Figure 9). It is also observed that increasing TSS from 6 to 12 kg m^{-3} gives a reduction of J_{LIM} of 30% for shear stress in the range 3–9 Pa. The higher concentration gives lower J_{LIM} due to the $MLSS^{-0.5}$–term, but the higher concentration also influences J_{LIM} through a higher shear stress.

The higher J_{LIM} at higher rotation speed is a result of higher shear-induced diffusion. The lower J_{LIM} at higher TSS is ascribed to a lower concentration gradient between bulk feed and the accumulated foulants on the membrane, according to Eq. 2.

Using the proposed model for limiting flux as function of shear and concentration, the development of fouling layers can be simulated by a mass balance between permeation drag and back transport in terms of limiting flux, as proposed by Jørgensen et al. 2012. With this approach, the development in flux at different shear levels and concentrations can be determined. To increase performance of MBR filtration, the enhanced permeate production should balance the extraenergy required for creation of the additional shear to increase limiting flux.

Conclusions

The shear rate and shear stress on a rotating membrane disc in MBR sludge filtration was described as a function of rotation speed, radial distance and sludge concentration, by describing sludge as a non-Newtonian fluid.

An empirical model for the limiting flux as function of shear stress and sludge concentration was developed. The model was given two empirical parameters; a slope A depending on sludge characteristics (particle size, PSD, etc.) and an exponent B expressing the mechanistic influence of shear stress on limiting flux in the given system configuration.

The model was able to fit the experimental limiting fluxes for two different types of sludge, giving two different values of the empirical parameter A, reflecting the differences in sludge characteristics. The exponent B was constant through the experiments at different sludge characteristics. The variation in J_{LIM} as function of shear stress was documented by varying rotation speed and by measuring local flux as function of distance from center. Furthermore, the variation of J_{LIM} with concentration was documented from experiments on diluted and concentrated sludge. These variations in operational conditions were simulated well by the model.

The outcome of the study is a model that can predict the influence of increasing shear or sludge concentration on J_{LIM} for rotating disk filters.

Acknowledgments

This study is a part of the EcoDesign-MBR strategic research center. Special thanks to Grundfos Holding A/S and Grundfos BioBooster A/S for supporting this study.

Notation

a = Particle radius, m
A = empirical filtration constant, $kg^{0.5}{\cdot}m^{0.5}$ s^{-1}
B = empirical exponent for shear stress
CST = capillary suction time, s
D = diffusion coefficient
D^* = dimensionless hydrodynamic diffusion coefficient
D_S = shear-induced diffusion coefficient
D_B = Brownian diffusion coefficient
J = permeate flux, m s^{-1}
J_{LIM} = limiting flux, m s^{-1}
k = velocity factor
m = fluid consistency index
n = flow behavior index
P_a = characteristic pressure, Pa
r = radius, m
r_i = inner radius, m
r_o = outer radius, m
R^2 = coefficient of determination
Re = Reynolds number
t = time, s
TMP = transmembrane pressure, bar
TSS = total suspended solids, kg m^{-3}
u^* = superficial air velocity, m s^{-1}
x = axial coordinate, m

Greek letters

α = specific cake resistance, m kg^{-1}
α_0 = specific cake resistance at no pressure, m kg^{-1}

$\dot{\gamma}_m$ = shear rate on membrane, s^{-1}
δ = boundary layer thickness, m
ζ = zeta potential, mV
μ = dynamic viscosity of water, Pa·s
μ_a = apparent viscosity, mPa·s
τ_m = shear stress on membrane, Pa
υ = kinematic viscosity, $m^2\ s^{-1}$
ϕ = volume fraction of foulants
ϕ_b = volume fraction of foulants in bulk
ϕ_w = volume fraction of foulants at wall/membrane
φ = geometric hindrance factor
ω = amount of fouling, kg m^{-2}
ω_c = amount of cake, kg m^{-2}
Ω = rotation speed, rpm, rad s^{-1}

Literature Cited

1. Drews A. Membrane fouling in membrane bioreactors—characterisation, contradictions, cause and cures. *J Membr Sci*. 2010;363:1–28.
2. Le Clech P, Chen V, Fane AG. Fouling in membrane bioreactors used for wastewater treatment. *J Membr Sci*. 2006;284:17–53.
3. Jiang T, Kennedy MD, Yoo C-K, Nopens I, van der Meer W, Futselaar H, Schippers JC, Vanrolleghem PA. Controlling submicron particle deposition in a side-stream membrane bioreactor: a theoretical hydrodynamic modelling approach incorporating energy consumption. *J Membr Sci*. 2007;297:141–151.
4. Meng F, Shi B, Yang F, Zhang H. New insights into membrane fouling in submerged membrane bioreactor based on rheology and hydrodynamics concepts. *J Membr Sci*. 2007;302:87–94.
5. Meng F, Yang F, Shi B, Zhang H. A comprehensive study on membrane fouling in submerged membrane bioreactors operated under different aeration intensities. *Sep Purif Technol*. 2008;59:91–100.
6. Shimizu Y, Okuno Y-I, Uryu K, Ohtsubo S, Watanabe A. Filtration characteristics of hollow fiber microfiltration membranes used in membrane bioreactors for domestic wastewater treatment. *Water Res*. 1996;30:2385–2392.
7. Tardieu E, Grasmick A, Geaugey V, Manem J. Influence of hydrodynamics on fouling velocity in a recirculated MBR for wastewater treatment. *J Membr Sci*. 1999;156:131–140.
8. Aubert M-C, Elluard MP, Barnier H. Shear stress induced erosion of filtration cake studied by a flat rotating disk method. Determination of the critical shear stress of erosion. *J Membr Sci*. 1993;84:229–240.
9. Wu G, Cui L, Xu Y. A novel submerged rotating membrane bioreactor and reversible membrane fouling control. *Desalination*. 2008; 228:255–262.
10. Bacchin P, Aimar P, Field RW. Critical and sustainable fluxes: theory, experiments and applications. *J Membr Sci*. 2006;281:42–69.
11. Huismann I, Trägårdh G, Trägårdh C. Particle transport in crossflow microfiltration: II. Effects of particle-particle interactions. *Chem Eng Sci*. 1999;54:281–289.
12. Jørgensen MK, Bugge TV, Christensen ML, Keiding K. Modeling approach to determine cake buildup and compression in a high-shear membrane bioreactor. *J Membr Sci*. 2012;409–410:335–345.
13. Bugge TV, Jørgensen MK, Christensen ML, Keiding K. Modeling cake buildup under TMP-step filtration in a membrane bioreactor: cake compressibility is significant. *Water Res*. 2012;46:4330–4338.
14. Bouzerar R, Ding L, Jaffrin M. Local permeate flux-shear-pressure relationships in a rotating disk microfiltration module: implications for global performance. *J Membr Sci*. 2000;170:127–141.
15. Jaffrin MY. Dynamic Shear-enhanced membrane filtration: a review of rotating disks, rotating membranes and vibrating systems. *J Membr Sci*. 2008;324:7–25.
16. Davis RH, Sherwood JD. A similarity solution for steady-state crossflow microfiltration. *Chem Eng Sci*. 1990;45:3203–3209.
17. Lee Y, Clark MM. A numerical model of steady-state permeate flux during cross-flow ultrafiltration. *Desalination*. 1997;109: 241–251.
18. Zydney AL, Colton CK. A concentration polarization model for the filtrate flux in cross-flow microfiltration of particulate suspensions. *Chem Eng Commun*. 1986;47:1–21.
19. Leighton DT, Acrivos A. The shear-induced migration of particles in concentrated suspensions. *J Fluid Mech*. 1987;181:415–439.
20. Laera G, Giordano C, Pollice A, Saturno D, Mininni G. Membrane bioreactor sludge rheology at different solid retention times. *Water Res*. 2007;41:4197–4203.
21. Pollice A, Giordano C, Laera G, Saturno D, Mininni G. Physical characteristics in a complete retention membrane bioreactor. *Water Res*. 2007;41:1832–1840.
22. Ratkovich N, Horn W, Helmus FP, Rosenberger S, Naessens W, Nopens I, Bentzen TR. Activated sludge rheology: a critical review on data collection and modelling. *Water Res*. 2013;47: 463–482.
23. Rosenberger S, Kubin K, Kraume M. Rheology of activated sludge in membrane bioreactors. *Eng Life Sci*. 2002;2:269–275.
24. Samuelsson G, Huismann IH, Trägårdh G, Paulsson M. Predicting limiting flux of skim milk in crossflow microfiltration. *J Membr Sci*. 1997;129:277–281.
25. Ducom G, Puech FP, Cabassud C. Air sparging with flat sheet nanofiltration: a link between wall shear stress and flux enhancement. *Desalination*. 2002;145:97–12.
26. Huismann IH, Trägårdh C. Particle transport in crossflow microfiltration–I. Effects of hydrodynamics and diffusion. *Chem Eng Sci*. 1999;54:271–280.
27. Belfort G, Davis RH, Zydney AL. The behavior of suspensions and macromolecular solutions in crossflow microfiltration. *J Membr Sci*. 1994;96:1–58.
28. Jönsson AS. Influence of shear rate on the flux during ultrafiltration of colloidal substances. *J Membr Sci*. 1993;79:93–99.
29. Ding L, Al-Akoum O, Abraham A, Jaffrin MY. Milk protein concentration by ultrafiltration with rotating disk modules. *Desalination*. 2002;144:307–311.
30. Ghogomu JN, Guigui C, Rouch JC, Clifton MJ, Aptel P. Hollow-fibre membrane module design: comparison of different curved geometries with Dean vortices. *J Membr Sci*. 2001;181:71–80.
31. Moll R, Veyret D, Charbit F, Moulin P. Dean vortices applied to membrane process Part I: experimental approach. *J Membr Sci*. 2007:288;307–320.
32. Rashaida AI. Flow of a Non-Newtonian Bingham Plastic Fluid Over a Rotating Membrane Disc. PhD Thesis. University of Saskatchewan, Saskatoon, Saskatchewan, 2005.
33. Ratkovich N, Chan CCV, Bentzen TR, Rasmussen MR. Experimental and CFD simulation of wall shear stress for different impeller configurations and MBR activated sludge. *Water Sci Technol*. 2012; 65:2061–2070.
34. Field RW, Wu JJ. Modelling of permeability loss in membrane filtration: re-examination of fundamental fouling equations and their link to critical flux. *Desalination*. 2011;283:68–74.

Manuscript received Oct. 1, 2013, and revision received Oct. 23, 2013.